AUT Journal of Civil Engineering

AUT J. Civil Eng., 5(3) (2021) 433-448
DOI: 10.22060/ajce.2022.19395.5729

Modified Dynamic Stress Concentration Factor for the Scattering of P-wave by Twin Tunnels

A. Rabiefar[1], H.R. Vosoughifar[2]*, A. Nabizadeh[3], H. Negahdar[1]

[1] Department of Civil Engineering, Faculty of Civil and Earth Resources Engineering, Central Tehran Branch, Islamic Azad University, Tehran, Iran
[2] Department of Civil Engineering, South Tehran Branch, Islamic Azad University, Tehran, Iran
[3] Department of Civil Engineering, Shahid Rajae Teacher Training University, Lavizan, Tehran, Iran

ABSTRACT: Stress concentration around twin tunnels and its impact on monuments have been receiving much attention from researchers. To investigate the effect of scattering in twin tunnels, the Hankel function of the first kind has been used by various researchers. The mathematical relation of Fourier expansion was modified and the time-domain analysis was transformed to frequency-domain analysis to provide a novel method for analyzing stress concentration factors. The combined finite element scattering model (FESCAM) was designed and developed in MATLAB. Analysis was performed in the presence of twin tunnels with a scattering of P-wave and in the absence of twin tunnels under the effect of a near-field earthquake. According to the results, dynamic stress concentration factor (DSCF) for Kobe earthquake P- wave with different wave angles and maximum frequency showed maximum scattering at $\alpha=0°$ and $\theta=0°$ in the tunnel. In addition to the increased stress concentration factor, the results of the Mann-Whitney statistical test in SPSS revealed a significant difference between the seismic performance of Arg-e Karim Khani and Zand underpass in the presence and absence of the tunnel (P Value<0.05). A scattering effect of less than 10% was calculated taking into account the combined effect of the calculated seismic waves using incremental extended finite element software. Scattering depends on frequency, and higher scattering was reported for higher frequencies.

Review History:

Received: Dec. 16, 2020
Revised: Mar. 29, 2021
Accepted: Jan. 26, 2022
Available Online: Jan. 31, 2022

Keywords:

Monument
Twin tunnels
Dynamic
Wave scattering
Time history

1- Introduction

Underground structures such as tunnels have been increased as a result of population growth in large cities. Earthquake waves such as longitudinal and shear waves may affect rapidly on underground structures, it leads to different displacements on the adjacent structures. For this purpose, many researchers investigated the impact of earthquake damages on tunnels. It is so important to evaluate the effect of underground structures such as tunnels whether during excavation or significantly during an earthquake on the adjacent structures. This becomes even more important when considering the immense material and immaterial values of historic structures [1-3]. There are almost 40 cultural heritage properties that have severe damage in the Seismic areas of Iran. If an earthquake wave collides to an underground cavity such as a tunnel, it redirects because of the soil profile while some part of the wave is emitted into the environment this phenomenon is called scattering [4]. Mow and Pao (1973) were a pioneer in investigating the scattering of waves around a cylinder in an unlimited environment [5]. Manolis (1980) examined the dynamic behavior of uncoated underground structures with considering the impact of wave scattering applying the boundary element method. Manolis and Beskos (1983) studied the shape of the scattering of waves with considering the boundary limits [6, 7]. The scattering of p and SV waves was studied in a disparate environment at the Los Angeles basin [8]. A model for acoustic resistance according to the dimensionless frequency function through Bessel's equations and complex functions presented for the scattering of harmonic waves within a saturated pro-elastic ambience. 9]]. In this study, a 2D analytical solution for scattered and reflected P-waves in a saturated medium was proposed in cylindrical valleys based on Biot's dynamical theory [10]. An analytical solution was evaluated for the scattering of waves by a circular tunnel in an anisotropic, porous, elastic environment. The presented method solved the Biot equations by considering both complex functions for the solid and fluid frameworks on the 2D plane [11]. The effect of harmonic plane waves on a circular parallel tunnel of unlimited length was studied in a saturated pro-elastic environment. This research investigated the wave expansion equations through Biot's theory in pro-elastic environments and appropriate boundary conditions in cylindrical coordinates [12]. A method to solve the dynamic response of a cylindrical cavity in an infinite anisotropic porous environment was introduced based on the stabilized Biot's equations on the complex plane [13]. The dynamic stress factor in twin tunnels was investigated inside the saturated environment. This study noticed the type of materials, the frequency of waves, drainage conditions,

*Corresponding author's email: vosoughi@hawaii.edu

and proximity of the two tunnels on the linear stress. The results are illustrated through numerical examples in two tunnels with concrete coating located inside the saturated environment regarding the effect of wave scattering at different frequencies on the response curves [14]. In this research, a new approximation for the two-dimensional scattering of planar waves on a cylindrical cavity with the pro-elastic coating is presented based on the Biot equations and complex variables. The results showed that the tunnel's coating gets thicker generally at low frequencies and the shear modulus ratio at low frequencies increased [15]. Many researchers examined the effect of seismic waves on adjacent historic structures without considering scattering waves on twin tunnels. Some important research is given regarding scattering waves [16-20]. An analytical solution for the dynamic stress concentration of circular twin tunnels presented against vertical and shear waves in a filled space using derivatives of complex variables. The results illustrated the main effect on the dynamic response of the walls of the tunne [21]. The theory of complex variables on the plane and the visual method was applied s to present an analytic solution for the longitudinal (P-wave), shear (SV-wave), and Rayleigh harmonic wave scattering inside a shallow circular tunnel in a semi-elastic environment. The behavior of boundary conditions within the semi-elastic space and the tunnel walls were noticed. The parametric studies of this method mention the important effect of the tunnel alignment depth, shear modulus and thickness of the tunnel's coating on the dynamic responses [22]. The further researches used Helmholtz equations to investigate the scattering of SH waves in a circular tunnel with considering the granulated materials, the complex variable function was employed to examine the stresses and displacements in a circular tunnel and twin tunnels [23]. The scattering of seismic waves and tunnel's coating with considering the impact of stress concentration were illustrated by [24] The complex functions and structural mapping techniques and dynamic stress concentration were evaluated in granulated material for dynamic analysis of two cavities [25]. The harmonic waves scattering such as longitudinal (P-wave), shear (SV-wave), and Rayleigh were studied in an irregular layered medium. This research investigated the effects of scattering and seismic reflection using the weighted residual method. Their results demonstrated the scattered waves increased in different parts of the layer surfaces while decreasing in other parts [26]. Two-dimensional boundary conditions were applied in an elastic half-space around semicircular canyons for both longitudinal (P-wave), shear (SV-wave). Therefore, they simulated dimensionless stress boundary conditions in a half-space canyon. By using the extended Fourier method, the results showed that the cylindrical wave functions can be defined under dimensionless stress boundary conditions in a semi-circular space [27]. The seismic behavior of circular tunnels considering shear waves (P-wave) was investigated by a quasi-static analysis. Based on the results the propagation of shear waves caused elliptical deformations in circular tunnels [28]. The seismic response of P and SV waves of a linear poroelastic medium was applied in a nonlinear buried tunnel. According to the results, the magnitude of displacements around the tunnel increased at large periods [29]. In this study, the unstable wave dispersion distribution at the neutral axis of several cavities near the ground level was investigated. For this purpose, the weighted-residuals method was used to examine the scattering and dispersion of Riley, P, and SV surface waves around various layers and intensified ground motions in a heterogeneous environment. (i.e., diagonal angle to the axis of the cylinder), the diffracted wave was non-polar, where the spatial distribution was three-dimensional [30]. Developed mathematical models and novel code were studied for scattering. In this way, The values of displacement and DSCF of the monument were evaluated with and without considering the tunnels when the study domain is subjected to near-field earthquakes. The results indicated that the displacement of tunnels is less than adjacent structures during an earthquake [31]. By using the indirect boundary integral equation method the scattering of P, SV waves by the twin lining tunnels studied in an elastic half-space. According to the results, in high frequency the effect of stiffness coefficient on the displacement amplitude are bigger than low frequency [32]. A theoretical method investigated the incident SH waves to response of the two bonded semi-infinite medium with respective symmetrical circular cavities. In this way, the wave propagation equation is solved in the light of the wave function expansion method. The results illustrated that the interface displacements for low incident angle are bigger than high incident [33]. Based on the wave function expansion methods and Fourier transform the dynamic stress concentration around a circular cavity presented according to cylindrical P-waves. The results showed that the incident stress wave present significant effects on the dynamic response of a circular cavity [34]. The current study used the first kind of Hankel's function to analyze the input waves and compute the function of diffracted waves. Finally, a numerical analysis was conducted through dynamic stress concentration factor (DSCF) and the related graphs.

2- Methodology

2- 1- Hankel's equations

For the P-wave with an amplitude of $\varnothing_0$ emitted diagonally into the space according to Eq. (1), the initial potential of wave and the reflected wave potential of P-wave are calculated through $\varnothing^i$ ،$\varnothing^r$ respectively [22]:

$$\phi^i = \phi_0 \exp\left[ik_{L1}(x\sin\gamma + \gamma\cos\gamma)\right]$$
$$\phi^r = \phi_0 \exp\left[ik_{L1}(x\sin\gamma - \gamma\cos\gamma)\right] \quad (1)$$

In Eq. (1), A_1 and A_2 are the boundary conditions discussed later in another section. According to the propagation angle, γ, critical propagation angle, θ_{cr} is defined as follows [22]:

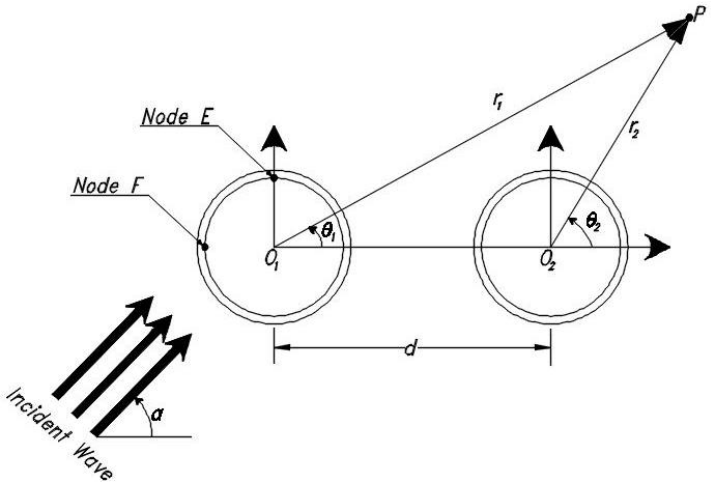

Fig. 1. Twin tunnels and effective parameters on wave scattering.

$$\theta_{cr} = \arcsin(1/k)\ ,\quad k_{L1} = \frac{C_{L1}}{C_{T1}} \tag{2}$$

In Eq. (2), k_{l1} is the ratio of length to width wave velocity under the Helmholtz theory, any vector field can be expressed as the total gradient of a scalar field and curl of a vector field. [35] Therefore, the displacement field of an infinite environment can be described through the wave equations according to Eq. (3) [12]:

$$\nabla^2\phi_{f,s} + k_{f,s}^2\phi_{f,s} = 0\ ,\quad \nabla^2\psi + k_t^2\psi = 0 \tag{3}$$

In Eq. (3), $\varphi_{f,s}$ is the potential function of fast and slow waves and k_f, k_s, and k_t are respectively the selected wave number in fast, slow, and shear elastic modes. The mentioned values are provided according to Eq. (4):

$$k_t^2 = \frac{c}{\mu(\rho_{22}\omega^2 + i\omega b)}\ ,$$

$$k_{f,s}^2 = \frac{B \pm \sqrt{B^2 - 4AC}}{2A} \tag{4}$$

$$M = \frac{1}{\left[(\beta-\phi_0)/k_s + \phi_0/k_{F1}\right]}\ ,$$

$$Q = \phi_0 M(\beta - \phi_0)$$

$$R = \phi_0^2 M\ ,\quad A = (\lambda + 2\mu)R - Q^2$$

$$B = \omega^2\left[\rho_{11}R + \rho_{22}(\lambda+2\mu) - 2\rho_{12}Q\right] + i\omega b(\lambda + 2\mu + 2Q + R)$$

$$C = \omega^2\left[\omega^2(\rho_{11}\rho_{22} - \rho_{12}^2) + i\omega\rho b\right]$$

In Eq. (4), values of ρ_{11}, ρ_{22} and ρ_{12} are the effective densities (independent of frequency), ω is the frequency of stimulation, ε_0 is porosity, K_s is bulk modulus of elastic materials, K_{F1} is the bulk modulus of saturated fluid, μ is the shear modulus and λ is the Lame's first parameter [12]. Taking into account the scattering, based on the above equations, the considered range has been shown in Fig. 1.

The dynamics of scattering are expressed through Fourier's series. The fast and slow waves in the coordinates system of each cylindrical cavity are expressed according to Eq. (5) [12]:

$$\phi_{f,s}^{(i)} = \sum_{n=-\infty}^{\infty}\gamma_n^{(i)} J_n(k_{f,s}r_i)e^{in\theta_i}\ ,\ i = 1,2$$
$$\gamma_n^{(1)} = i^n e^{-in\alpha}\ ,\quad \gamma_n^{(2)} = \gamma_n^{(1)} e^{ikd\cos\alpha} \tag{5}$$

In Eq. (5), J_n is the Bessel function of first kind for the cylindrical environment. Similarly, the scattering potential around the cavities in pro-elastic environment is expressed

by Eq. (6) [12]:

$$\begin{aligned}\phi_f^{(i)} &= \sum_{n=-\infty}^{\infty} A_n^{(i)}(\omega) H_n(k_f r_i) e^{in\theta_i} \ , \\ \phi_s^{(i)} &= \sum_{n=-\infty}^{\infty} B_n^{(i)}(\omega) H_n(k_s r_i) e^{in\theta_i} \\ \psi^{(i)} &= \sum_{n=-\infty}^{\infty} C_n^{(i)}(\omega) H_n(k_t r_i) e^{in\theta_i}\end{aligned} \tag{6}$$

In Eq. (6), H_n is the Bessel function of first kind is cylindrical. Hence, the total potential function in the pro-elastic environment around the cylindrical cavities for interaction of multiple scatterings is initially formulated as follows [12]:

$$\begin{aligned}&\phi = \phi_f^{(i)} + \phi_s^{(i)} + \phi_f^{(j)} + \phi_s^{(j)} + \phi_{f,s}^{(j)} \\ &\phi = \sum_{n=-\infty}^{\infty} A_n^{(i)}(\omega) H_n(k_f r_i) e^{in\theta_i} + \\ &\sum_{n=-\infty}^{\infty} B_n^{(i)}(\omega) H_n(k_s r_i) e^{in\theta_i} + \\ &\sum_{n=-\infty}^{\infty} \gamma_n^{(i)} J_n(k_{f,s} r_i) e^{in\theta_i} + \ldots + \\ &\sum_{n=-\infty}^{\infty} [A_n^{(j)}(\omega) H_n(k_f r_j) + B_n^{(j)}(\omega) H_n(k_s r_j)] e^{in\theta_i} \\ &\psi = \psi^{(i)} + \psi^{(j)} = \sum_{n=-\infty}^{\infty} \left[C_n^{(i)}(\omega) H_n(k_t r_i)\right] e^{in\theta_i} + \\ &\sum_{n=-\infty}^{\infty} \left[C_n^{(j)}(\omega) H_n(k_t r_j)\right] e^{in\theta_i}\end{aligned} \tag{7}$$

In Eq. (7), $i, j = 1,2 (i \neq j)$ is true. In each equation, J is an index for expressing the Jth cavity in the Jth coordinate system. These conditions must be transferred to the coordinate system of ith cylinder before applying the boundary conditions. In Eq. (7), $A_n(\omega)$ and $B_n(\omega)$ are the boundary coefficients [12].

2- 1- 1- Boundary conditions

To determine the coefficients of $A_n(\omega)$ and $B_n(\omega)$ in Eq. (7), the boundary conditions and interaction environment conditions should be considered linear. The boundary conditions at ground level for free stress are expressed in Eq. (8) [22]:

$$\sigma_{y1} = \sigma_{xy1} = 0 \qquad (y = 0) \tag{8}$$

The boundary conditions for the stress of the tunnel's coating are expressed in Eq. (9).

$$\sigma_{r2} = \sigma_{r\theta 2} = 0 \qquad (r_1 = R_1) \tag{9}$$

The desirable boundary conditions at the surface of each cylindrical cavity lead to a unique solution to the problem expressed according to Eq. (10) [12]:

$$\begin{aligned}&\sigma_{rr}^{(i)}\Big|_{r_{i=a,b}} = 0 \ , \quad \sigma_{r\theta}^{(i)}\Big|_{r_{i=a,b}} = 0 \ , \\ &w_r^{(i)}\Big|_{r_{i=a,b}} = k_s P_P^{(i)}{}_{r_{i=a,b}}\end{aligned} \tag{10}$$

In Eq. (10), $\dot{w}_r = \varnothing_0 (\dot{U}_r - \dot{u}_r)$ is the rate of filtration, U is the displacement of solid environment, u is the displacement of saturated fluid environment, and $0 \le k_s < \infty$ represents the permeability. Using the assumptions of Biot theory, Eq. (3) and simplification, Eq. (11) are provided as follows [14]:

$$\begin{aligned}&P_p = Mb_f K_f^2 \phi_f + Mb_s K_s^2 \phi_s \ , \\ &\sigma_{rr} = a_f k_f^2 \phi_f + a_s k_s^2 \phi_s + 2\mu u_r \\ &\sigma_{r\theta} = \frac{\mu}{r}\left(\frac{\partial u_r}{\partial \theta} + r\frac{\partial u_\theta}{\partial r} - u_\theta\right), \\ &\sigma_{\theta\theta} = a_f k_f^2 \phi_f + a_s k_s^2 \phi_s + 2\mu\left(\frac{u_r}{r} + \frac{1}{r} u_\theta\right)\end{aligned} \tag{11}$$

In Eq. (11), σ_{rr} is normal stress, $\sigma_{r\theta}$ is tangential stress, $\sigma_{\theta\theta}$ is cyclic stress and P_p is fluid pore pressure. The values of $a_{f,s}$ and $b_{f,s}$ are expressed in Eq. (12) [14]:

$$\begin{aligned}a_{f,s} &= -\lambda_f + \phi_0 \beta M_0 (1 - \mu_{f,s}) \ , \\ b_{f,s} &= \beta + \phi_0 (\mu_{f,s} - 1)\end{aligned} \tag{12}$$

In Eq. (12), the values of $\mu_{f,s}$ and λ_f are calculated based on Eq. (13) [9]:

Table 1. Specifications of scaled near-field accelerograms.

Earthquakes	Year	Station	Magnitude	PGA (g)	R_{rup}(km)
Northridge	1994	Anacapa Island	6.69	1.2919	20.72
Tabas	1978	Boshrooyeh	7.35	0.4301	28.79
Kobe	1995	Abeno	6.9	0.9340	24.85

Table 2. Frequency domain data of selected earthquakes.

Frequency	Fourier Amplitude (Northridge)	Fourier Amplitude (Tabas)	Fourier Amplitude (Kobe)
0.1	0.234	0.030	0.028
1	0.129	0.038	0.12
10	0.014	0.073	0.029

$$\lambda_f = k_f - \frac{2\mu}{3},$$
$$\mu_{f,s} = \frac{\omega^2(\rho_{11}R - \rho_{12}Q) - k_{f,s}^2\left[(\lambda+2\mu)R - Q^2\right] + J\omega b(Q+R)}{\omega^2(\rho_{22}Q - \rho_{12}R) + J\omega b(Q+R)} \quad (13)$$

This study involved the non-linear time history analysis to generalize Hankel Equation and accurately calculate the scattering. The input waves examined by the researchers were applied for Hankel's function of harmonic waves, while the seismic waves are inherently based on time history. After the analysis stage, the Fourier was applied to transform the time solution environment into frequency environment. Then, the dominant frequencies were evaluated in the Hankel's function. The time span was transformed into frequency based on Eq. (14):

$$a(t_k) = \sum_{n=-\frac{N}{2}}^{\frac{N}{2}-1} F(\omega_n).\exp(i\omega_n t_k) \quad (14)$$

In Eq. (14), $a(t_k)$ is the value of acceleration time history at t_k. Moreover, $F(\omega_n)$ is the discrete Fourier transform at frequency of ω_n, while N is the degree of Discrete Fourier Transform. Fig. 2 provides the extended finite element program. As illustrated in the flowchart, the mathematical equations were employed to describe the level of displacement and stress through the Biot theory and the initial conditions of the case study. The potential of input waves is defined through Hankel's function Porosity Value ϕ_0 in the model was considered dependent on the supplemental frequency, which was extended to frequency range through Eq. (15) [36]:

$$C_L = \sqrt{\lambda_e + 2\mu_e/\rho_e},$$
$$C_T = \sqrt{\mu_e/\rho_e}, \quad (15)$$
$$\rho_e = (1-\phi_0)\rho_s + \phi_0\rho_{fl}$$

Where C_L, C_T and ρ_e are the coefficients of the fast shear wave, shear wave velocity, and average density in the elastic environment, respectively [12]. Whereas the frequency domain is needed to study the scattering of waves, the seismic harmonic wave was transferred to the frequency domain using the Fourier expansion. Using the code written in MATLAB (FESCAM), the scattering of waves around the twin tunnels was investigated. Dynamic stress concentration factor (DSCF) was introduced as a dimensionless parameter to study the scattering of waves. Displacement was calculated by the finite element program. Displacement was examined in the presence and absence of a tunnel with the scattering of waves. Fig. 2 shows the algorithm. Different angles were studied using the developed program. The characteristic feature of the code written in MATLAB (FESCAM) is the investigation of wave scattering using accelerographs or frequencies scaled for earthquakes in Table 1.

2- 2- Accelerogram of the earthquake

Because of the study area, Tabas, Northridge, and Kobe near-field earthquakes were selected. According to the Iranian Code of Practice for Seismic Resistant Design of Buildings [37]. Shiraz is among the areas with relatively high seismicity. Thus, the accelerographs should be modified to 0.3 g. regarding the characteristics of the soil in the case study, three earthquakes were selected. The specification of a selected earthquake is shown in Tables 1 to 3 display the applied frequencies that performed Fourier transforming function the time domain data of selected earthquakes [38].

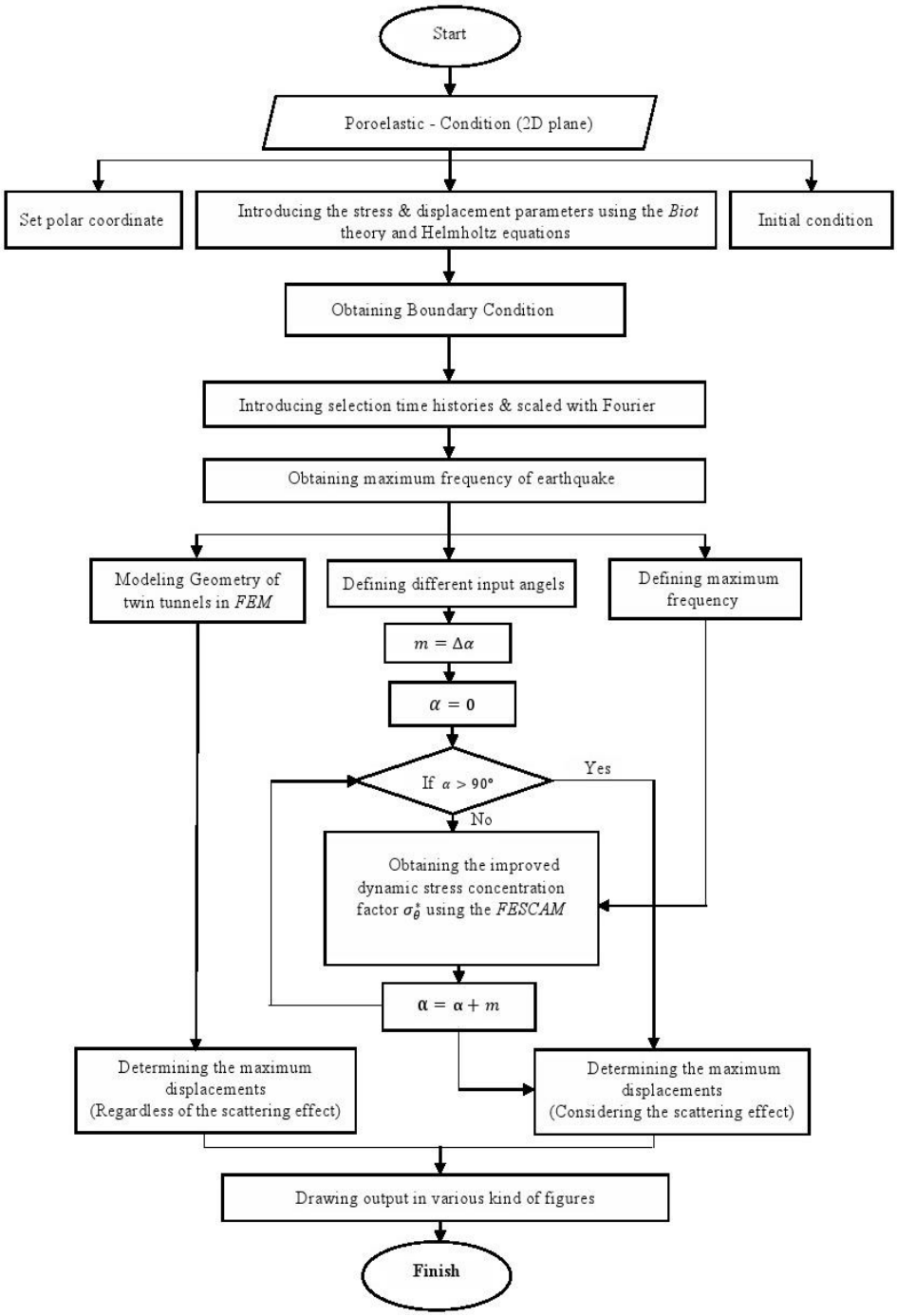

Fig. 2. Optimized flowchart for the scattering code.

Table 3. The maximum frequency of selected earthquakes.

Earthquakes	Frequency$_{(Peak\ Acceleration)}$	Fourier Amplitude
Northridge	3.394	0.276
Tabas	6.714	0.810
Kobe	7.251	0.095

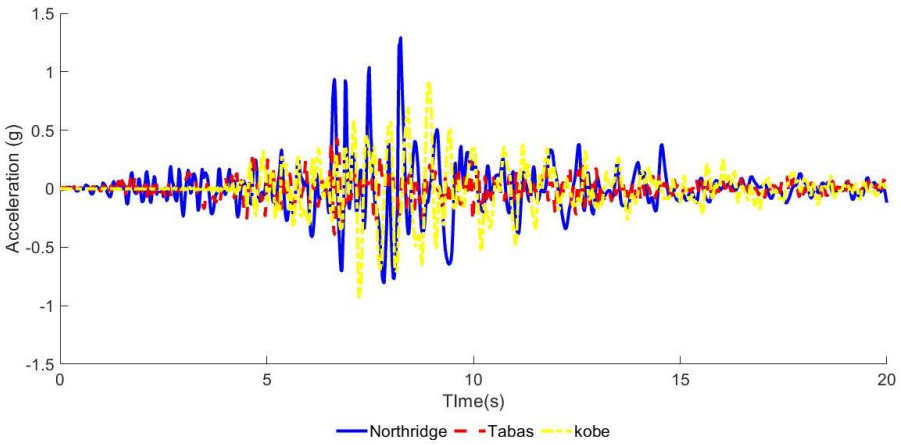

Fig. 3. Accelerograms for the three near-field earthquakes (Northridge, Tabas, and Kobe).

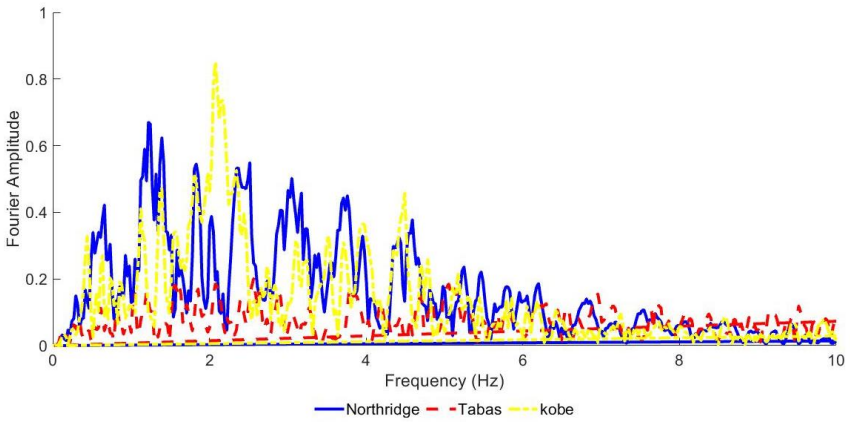

Fig. 4. Fourier spectrum for the three near-field earthquakes (Northridge, Tabas, and Kobe)..

Using the above equation, the scaled accelerograms displayed in Fig. 3, the Fourier spectrum of the earthquake can be seen in Fig. 4 [38].

The main feature of the developed program FESCAM with the past studies is the application of frequency spectrum scaled for the seismic waves rather than the harmonic waves. To achieve this objective, there frequencies that correspond to the beginning, end, and the maximum amplitude of Fourier, are shown in Table 2. The value of the maximum frequency that occurred during an earthquake shows in Table 3.

2- 3- Arg-e Karim khani structure adjacent to twin tunnels (Shiraz, Iran)

A section of Shiraz Subway Line 1 near Arg-e Karim Khani with a length of 24.1 km and a diameter of 6 m was selected as the study area. Arg-e Karim Khani was the royal palace and andaruni of Karim Khan, the governor of Shiraz. It was built in 1180 A.H. by the order of Karim Khan in an area of 12,800 m^2 with a building area of about 4000 m^2 in northeastern Shiraz [39]. The section selected for the research is where the twin tunnels of Shiraz Subway with a length of

Table 4. Geotechnical parameters of the tunnel and Arg-e Karim Khani structure.

Soil Layer	Layer's thickness (m)	γ_{sat} (kg/m^3)	E (kg/m^2)	ν	φ	ψ	C (kg/m^2)
Clayey sand	4.0	1900	$10^5\times 32.5$	0.30	33	0.1	3000
Clay sediment	3.2	2080	$10^5\times 50$	0.25	29	0.15	4000
Compressed silt	6.7	2090	$10^5\times 30$	0.25	32	0.1	1000
Compressed clay	3.0	2080	$10^5\times 50$	0.25	29	0.1	2000
Clay sediment	1.8	2090	$10^5\times 50$	0.25	32	0.15	1000
Silty sand	21.3	2090	$10^5\times 50$	0.25	29	0.1	1000

Table 5. Coordinate selected nodes on Arg-e Karim Khani and tunnel

Node	X (m)	Y (m)
A	95.29	40.00
B	104.40	40.00
C	194.40	40.00
D	205.80	40.00
E	243	21.00
F	239	17.80

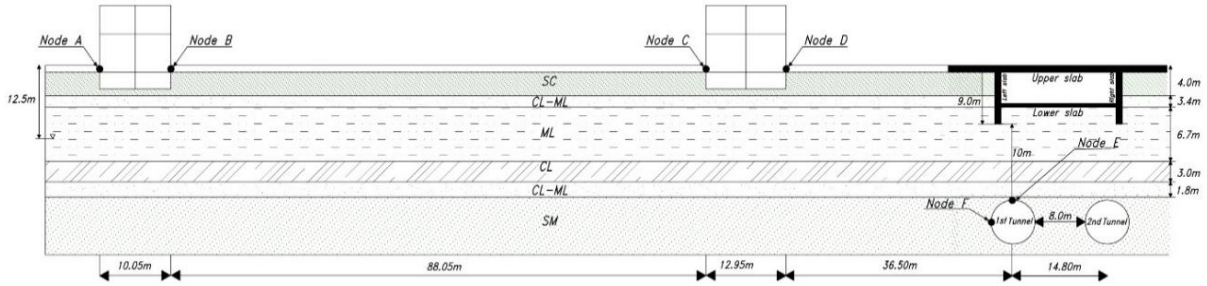

Fig. 5. The geometry of Arg-e Karim Khani.

about 1km pass from underneath such monuments as Arg-e Karim Khani, Pars monument, and Vakil Bazaar. The tunnel crown is located in the depth of approximately 10m. The specifications of the simulated model including the cross-section of Arg-e Karim Khani, tunnel distance from Arg-e Karim Khani, soil layers under Zand underpass, and the geometry of twin tunnels are listed in Tables 4 and 5. The center-to-center distance of the twin tunnels is 14.8 m with outer and inner diameters of 6.8 and 6 m, respectively. The thickness of the tunnel cover and the thickness and length of tunnel segments is 0.14, 0.3, and 1.4 m, respectively [16].

In Table 4, γ_{sat} is the saturation density, E is Young's modulus, ν is the Poisson's ratio, φ is the internal friction angle, ψ is the dilation angle and C is the soil adhesion.

As can be seen in Fig. 6, the placement of the twin tunnel is near the monument and in Fig. 7, the model meshing is shown in the finite element method program.

Fig. 6. The Arg-e Karim Khani and location of them near Zand underpass.

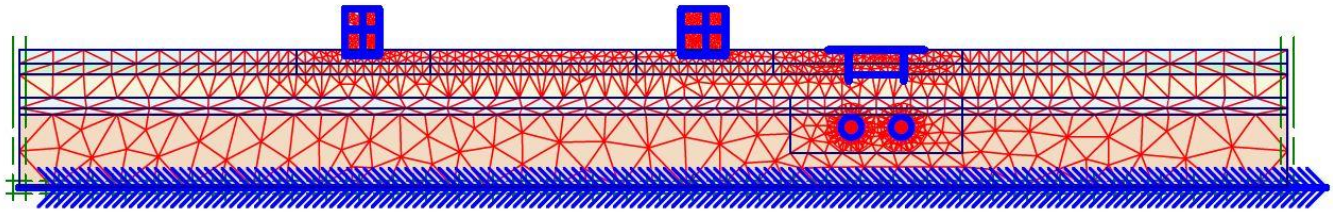

Fig. 7. The mesh grid in the FEM modeling.

3- Validation

3- 1- Developed code in MATLAB (FESCAM)

The validation process of the FESCAM code was performed by comparing the results of this study with the results of Hasheminejad et al. (2007). Figure 8 shows the scattering curves and the dynamic pressure concentration coefficient for the longitudinal input wave (P) at different frequencies. The incident wave angle and frequencies of this analysis were considered 60 degrees and 10, 100, 1000 Hz, respectively [12].

Since the wave energy has inversely correlated with its frequency, it tends to have higher wave energy at lower frequencies. Therefore, crossing the tunnel almost does not have any significant scattering. Conversely, high-frequency waves would experience more scattering due to hitting the walls of the tunnel. Fig. 8 shows the scattering in the wall of tunnels. There is not any significant difference between the result of FESCAM and Hasheminejad et al.'s research on applying harmonic waves as incident waves.

4- Results and Discussion

4- 1- Finite element method modeling

In this study, the advanced finite element method program (Plaxis) was used to model the twin tunnels and Arg-e Karim Khani structure in 2D plane coordinate. The FEM modeling was carried out in two steps: a) without twin tunnels and b) with twin tunnels. In this section, the software developed by finite element was used to examine the horizontal and vertical displacements of Arg-e Karim Khani under the earthquakes. The degrees of displacement with and without the involvement of the tunnel have been illustrated in Fig. 9. The effect of scattering was modeled through the expanded dimensionless parameter through the dynamic stress concentration factor (DSCF) provided in Eq. (12). According to the Biot Theory, the values required in the numerical analysis were imported into the extended model as can be seen in Table 6. The values of input frequencies were considered as input frequencies in FESCAM based on the non-linear time history analysis as shown in Table 2.

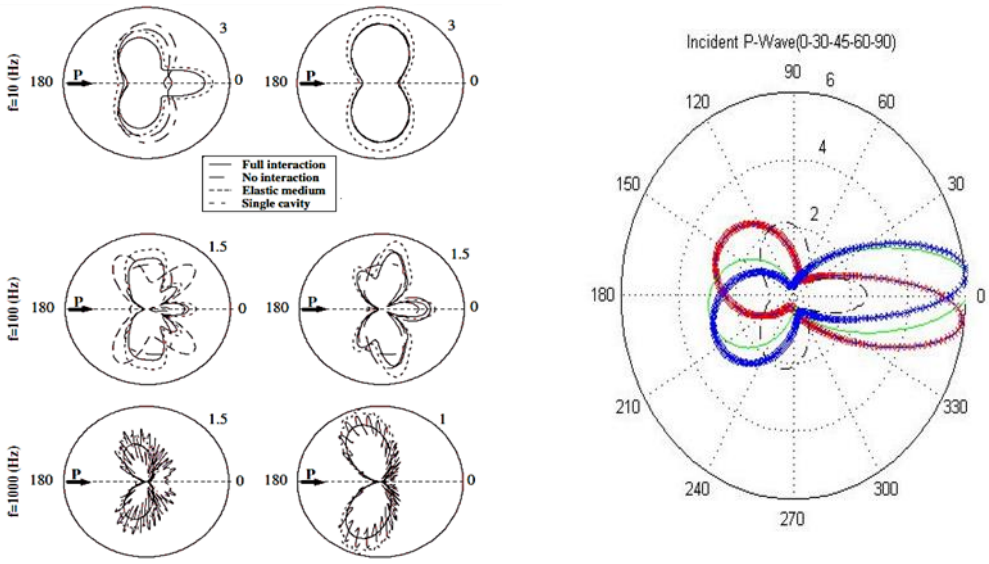

(a) Hasheminejad et al. (b) This study

Fig. 8. The Comparison between the results of Hasheminejad et al., and this study.

Table 6. The requirement parameters as input values for novel code.

Parameters	Saturated sand soil	Parameters	Saturated sand soil
α_∞	1.58	$\kappa\ (m^2)$	27.7×10^{-12}
$\rho_s(kg/m^3)$	2120	$K_s(N/m^2)$	4.99×10^{12}
$K_0(N/m^2)$	5.24×10^{11}	$\mu(N/m^2)$	3.26×10^{11}
$\rho_{fl}(kg/m^3)$	1000	$K_{fl}(N/m^2)$	2.25×10^{11}
$\eta(kg/m\ s)$	0.1	$\Lambda(m)$	19.4×10^{-6}

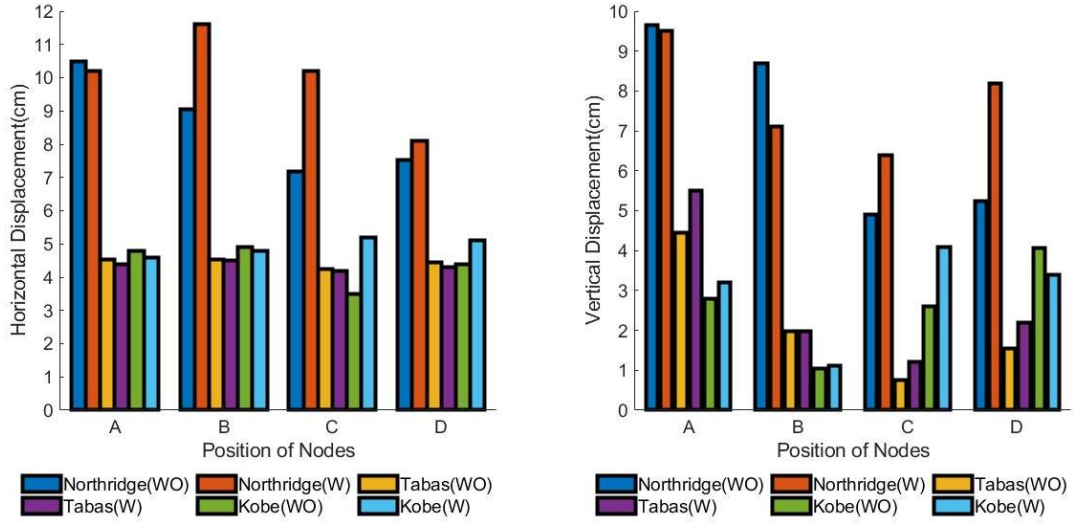

Fig. 9. Comparing displacement in the presence and absence of tunnels under near-field earthquakes.

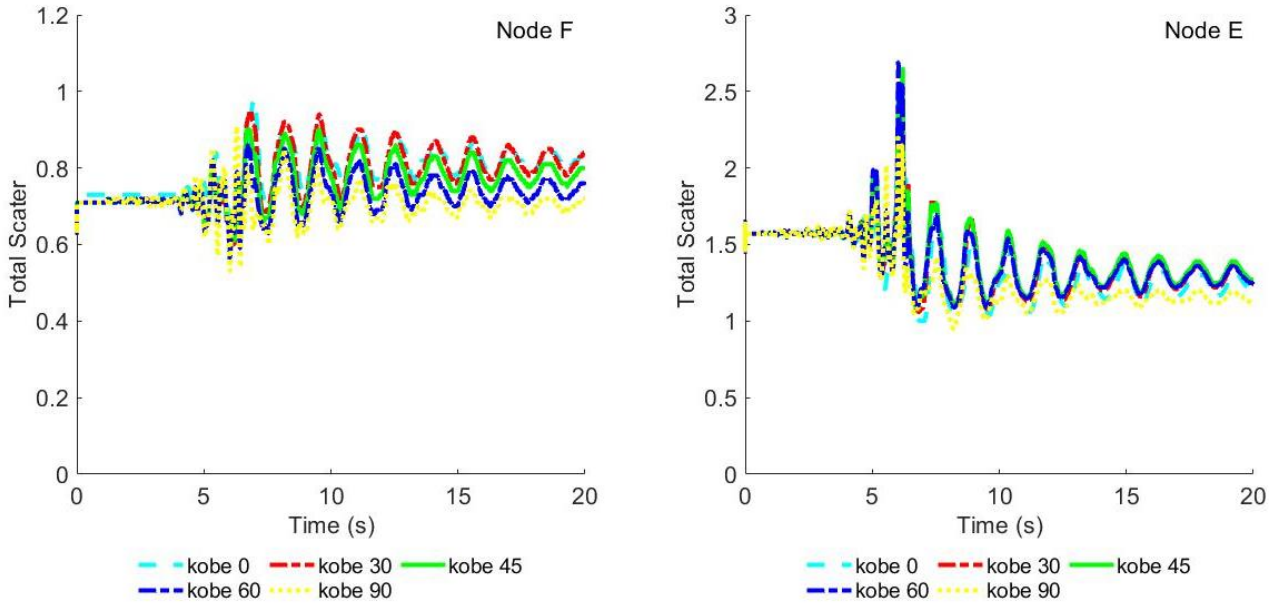

Fig. 10. Dynamic stress concentration factor for Kobe earthquake P- wave with different wave angles at Node E, Node F.

The center-to-center distance of the tunnels and Arg-e Karim Khani were, as provided in Fig. 5, ranged from d=44.2 m to d=154.71 m. The displacements were calculated at distances d=44.2, d=55.6 and d=145.6 m. Finally, d=44.2 m was selected as critical distance since the tunnel was closed to Arg-e Karim Khani and left a higher induction effect. The results have been presented in Fig. 9 [40].

To evaluate the effect of dimensionless dynamic stress concentration around the twin tunnels, FEM software was adopted. In this method, the improved dynamic stress concentration obtained from the radial stress (σ_{rr}) and cyclic stress $(\sigma_{\theta\theta})$. The dimensionless dynamic stress concentration factor is defined as Eq. (16) [34]:

$$\sigma_{\theta}^{*} = \frac{\sigma_{\theta\theta}}{\sigma_{rr}} \tag{16}$$

The dimensionless dynamic stress concentration factor values for Kobe earthquake P wave with different wave angles were examined as shown in Fig. 10.

According to Fig. 9, vertical and horizontal displacements in the presence and absence of tunnel for Kobe, Northridge, and Tabas earthquakes were studied using the finite element method [40]. As can be seen, the displacement is larger in the presence of a tunnel for all three earthquakes. Comparing the vertical and horizontal displacements, it is concluded that maximum horizontal and vertical displacements occurred in the Northridge earthquake. The results indicate that the vertical displacements are smaller than the horizontal ones. Given the geological characteristics and the slag weight of the tunnel and structure, this assumption is confirmed.

4- 2- FESCAM numerical analysis

The FESCAM numerical analysis was conducted to calculate dynamic stress concentration factor for comparing with the other results in the first kind of Hankel's function was used to analyze the input waves and calculate the function of scattering waves.

Figs. 10 and 11 show the dynamic stress concentration parameter for a longitudinal wave of Kobe earthquake with different wave angles and frequency at maximum wave power. As can be seen evidently in this Fig. 10, at the angle of $\alpha = 30°$, the greatest scattering took place at $\theta = 90^{\circ}$. Furthermore, the earthquake with input wave of $\alpha = 90^{\circ}$ and $\alpha = 60^{\circ}$ had the largest scattering values, respectively, at angles $\theta = 104^{\circ}$ and $\theta = 36^{\circ}$. Generally, the greatest values of scattering occurred at an angle of $\alpha = 30°$. However, the previous researchers better demonstrated the physics of the problem by considering the input wave angle $\alpha = 0^{\circ}$ for horizontal earthquakes and $\theta = 90^{\circ}$ for vertical earthquakes [12, 21]. Also, Fig. 10 (a) shows in P- wave earthquake with the incident angle of $\alpha = 30°$, the greatest scattering took place at $\theta = 90^{\circ}$.

The wave with input angles ($\alpha = 0^{\circ}$, $\alpha = 45^{\circ}$, $\alpha = 30°$

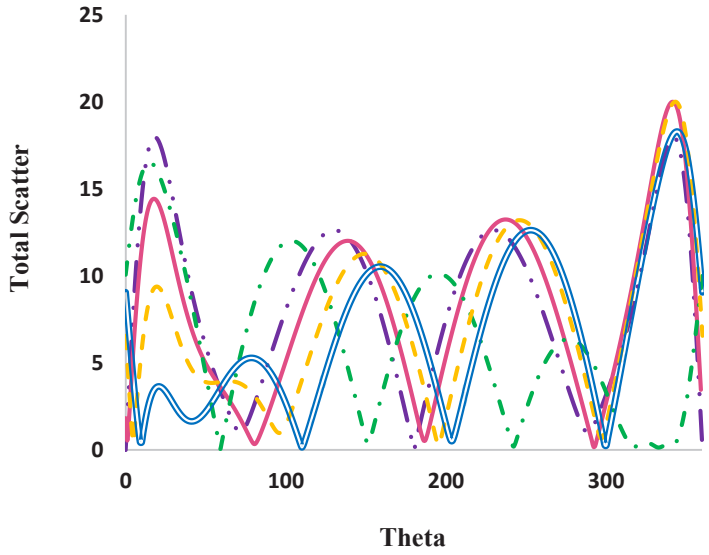

Fig. 11. DSCF for Kobe earthquake with different wave angles and frequency at maximum P-wave power.

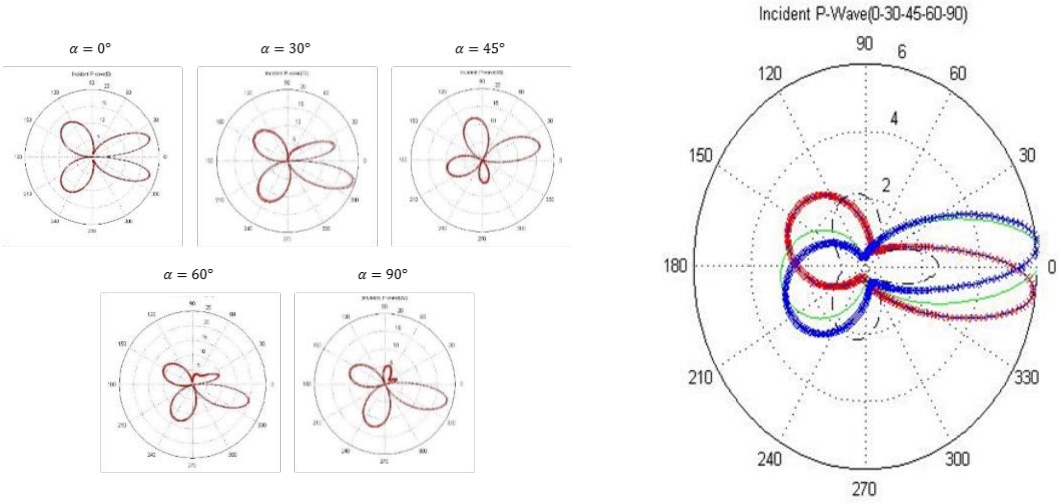

(a) Tabas and Kobe **(b) Northridge**

Fig. 12. DSCF for the longitudinal input wave (P) at different frequencies and input angles.

$\alpha = 60°$, and $\alpha = 90^{\circ}$) was applied on the left-hand tunnel through the developed version of FESCAM. Fig. 12 illustrates the dynamic stress concentration factor (DSCF) at a distance of 44.2 m. As is clear in the figures, the maximum value of scattering in the twin tunnels occurred under earthquake with input wavelength (p) of $\alpha = 30°$ at an angle ($\theta = 90^{\circ}$).

It was revealed that the viscosity effect dominates the internal layers at frequencies far lower than the critical frequency Biot ($f_{c=\varphi_0\eta/2\pi\rho_{fl}\kappa\alpha_\infty=1.35\times10^3\ Hz}$). For example, a linear flow (Poiseulle) occurs, while the boundary layer is much thicker than the core, where the viscous fluid leads to lock-on over the motion of the solid part. According to the results presented in Fig. 12, as the velocity of the wave increases the scattering rises at a slighter slope. Therefore, the Biot boundary frequency is transformed into a low-velocity frequency. In this scenario, fewer waves are emitted only within porous elastic environments [41].

Table 7. Statistical results of horizontal displacement of selected points at arg-e Karim Khani structure.

Independent samples Mann-Whitney U test			
Total N	**Mann-Whitney U**	**Wilcoxon W**	**P-value**
24	52.00	130.00	0.248

Table 8. Statistical results of vertical displacement of selected points at arg-e Karim Khani structure.

Independent samples Mann-Whitney U test			
Total N	**Mann-Whitney U**	**Wilcoxon W**	**P-value**
24	67.50	145.50	0.795

Table 9. The mean of horizontal and vertical displacements of monuments subjected to near-field earthquakes.

Mean displacement	Without tunnels (cm)	With tunnels (d=44.2 m) (cm)
$U_h(cm)$	4.45	5.10
$U_v(cm)$	5.25	3.40

4- 3- Statistical results

To compare the two data groups, the null hypothesis (H_0) is one of the most common ones in the nondifference problems. In other words, there is no difference between the degrees of the two groups. The Mann-Whitney in statistics is a nonparametric test used to measure the difference between the samples. The Mann-Whitney test is the nonparametric equivalent of the independent t-test applied for the comparison of data obtained from independent group schemes. This test is used when the conditions of using the parametric tests in the variables are not met, i.e., the variables are not continuous and normal, the variances of the two sets are not equal, and the ordinal and interval variables are smaller than 10. This study focused on two groups of displacements at Arg-e Karim Khani with and without the involvement of a tunnel. In calculating the value of the Mann-Whitney test, the comparisons are as many as the data of the first group (N_A) in the data of the second group (N_B) which is $N_A \times N_B$.

If the null hypothesis is true, then the value of the Mann-Whitney test should be around 0.5 (half hit value). The minimum value of this test is zero. The maximum possible value is equal to $\frac{N_A \times N_B}{2}$. The P-value or the calculated probability is the estimation of the likely rejection of the null hypothesis about the research question. When the hypothesis is true, it is often considered $\alpha = 0.05$. When the P-value is greater than 0.05, the null hypothesis is true, approximately one at specific modes. In this study, all of the above conditions have been displayed in Tables 7 and 8.

Tables 7 and 8 show that there is a significant difference between the mentioned scenarios for the mean of horizontal and vertical displacement of selected points in the Arg-e Karim Khani monument.

Table 9 shows the mean of horizontal and vertical displacements in the presence and absence of the tunnel for the mentioned earthquakes. As is clear from the table, the horizontal and vertical displacements when involving the tunnel are increased.

5- Conclusion

As shown in Fig. 12, Comparing the angles, it can be concluded that the maximum scattering effect for longitudinal P-waves occurred at input angles of 0° and 30°, and 0° and 90°, respectively. As expected, the scattering effect of seismic waves of Tabas and Kobe earthquakes with a frequency of 6.68 and 7.22 is more than the scattering caused by the Northridge earthquake waves with a maximum frequency of 1.97. This is indicative of the proper functioning of the proposed program. The scattering of P-wave under near-field earthquake was examined using mathematical relationships and a novel computer program. The proposed method provides a new view of the amplitude of the input seismic wave. According to this view, the study area is dynamically analyzed by several scaled near-field earthquakes. Then, the time domain is transferred to the frequency domain using the Fourier expansion to calculate the real stress concentration

factor. Previous studies only considered the effect of harmonic waves in dynamic analysis, assuming constant amplitude for the input seismic waves [14, 23]. Therefore, the new proposed FESCAM flowchart provides more accurate results consistent with the seismicity of the region. The numerical analysis method developed in this study is a new method for analyzing the scattering of near-field seismic waves in two-dimensional porous media. According to the results, the distance and diameter of tunnels and the type of the near-field earthquake in terms of frequency have a dramatic impact on the dynamic stress concentration factor (DSCF).

Acknowledge

The authors wish to thank Shiraz Urban Railway Company, and Cultural Heritage, Handicrafts, and Tourism Organization of Fars Province for their assistance during various stages of this study.

References

[1] A.B. Amorosi, D., Numerical modeling of the transverse dynamic of circular tunnels in clayey soils, Soil Dynamics and Earthquake Engineering, 29(6) (2009) 1059-1072.

[2] H.R. Vosoughifar, Rabiefar, A, Seismic effect of tunnel in the saturated ambience on surface structures subjected to near field earthquake, in: Vienna Congress on Recent Advances in Earthquake Engineering and Structural Dynamis, 2013.

[3] H.R. Vosoughifar, Rabiefar, A, The effect of increasing the angle of incidence of earthquake on tunnel in the saturated ambience on surface structures subjected to near and far field earthquake, in: 10th International Congress on Civil Engineering (ICCE), Tabriz, Iran.. 2015.

[4] G.-b. Liu, Xie, K.-h. & Liu, X., Dynamic response of a partially sealed tunnel in porous rock under inner water pressure, Tunnelling and Underground Space Technology, 25(4) (2010) 407-414.

[5] Y.H.M. Pao, C, The diffraction of elastic waves and dynamics stress concentrations., Soil Dynamic & Earthquake Engineering, 16 (1973) 111-118.

[6] G. Manolis, Dynamic response of underground structures, 1980.

[7] G.B. Manolis, D. E, Dynamic response of lined tunnels by an isoparametric boundary element method, Computer Methods in Applied Mechanics and Engineering, 36(3) (1983).

[8] N.D.T. Moeen-Varizi, M., scattering and diffraction of plane P and SV waves by two-dimensional inhomogeneities, Soil Dynamics and Earthquake Engineering, 7(4) (1988) 189-200.

[9] S.M.H. Hasheminejad, H, Radiation Loading of a Cylindrical Source in a Fluid-Filled Cylindrical Cavity Embedded Within a Fluid-Saturated Poroelastic Medium, Journal of Applied Mechanics, 69 (2002) 675-683.

[10] Z.L. Chenggang, W, Scattering of plane SV waves by cylindrical canyons in saturated porous medium., Soil Dynamics and Earthquake Engineering, 25(12) (2005) 981-995.

[11] B.E. Gatmiri, H, Scattering of Harmonic Waves by a Circular Cavity in a Porous Medium: Complex Functions Theory Approach, International Journal of Geomechanics, 7(5) (2007) 371-381.

[12] S.A. Hasheminejad, R, Harmonic wave diffraction by two circular cavities in a poroelastic formation, Soil Dynamics and Earthquake Engineering, 27(1) (2007) 29-41.

[13] B.E. Gatmiri, H, Wave scattering in cross-anisotropic porous media around the cavities and inclusions, Soil Dynamics and Earthquake Engineering, 28(12) (2008) 1014-1027.

[14] S.M.A. Hasheminejad, R, Dynamic Stress Concentrations in Lined Twin Tunnels within Fluid-Saturated Soil, Journal of Engineering Mechanics, 134(7) (2008).

[15] L.-F. Jiang, Zhoub, X.-L. & Wang, J.-H, Scattering of a plane wave by a lined cylindrical cavity in a poroelastic half-plane, Computers and Geotechnics, 36 (2009) 773-786.

[16] M. Afifipour, Sharifzadeh, M., Shahriar, K. & Jamshidi, H, Interaction of twin tunnels and shallow foundation at Zand underpass, Shiraz metro, Iran, Tunnelling and Underground Space Technology, 26(2) (2011) 356-363.

[17] M. Azadi, The Seismic Behavior of Urban Tunnels in Soft Saturated Soils, Procedia Engineering, 14 (2011) 2069-3075.

[18] S. Russo, Testing and modeling of dynamic out-of-plane behavior of the historic masonry façade of Palazzo Ducale in Venice, Italy, Engineering Structures, 46 (2013) 130-139.

[19] B.e.a. Sevim, Finite element model calibration effects on the earthquake response of masonry arch bridges, Finite Elements in Analysis and Design, 47(7) (2011) 621-634.

[20] Y.T. Didem Aktas, A, Seismic evaluation and strengthening of nemrut monuments, Journal of Cultural Heritage, 16(3) (2015) 381-385.

[21] Q.W. Liu, R., Dynamic response of twin closely-spaced circular tunnels to harmonic plane waves in a full space, Tunnelling and Underground Space Technology, 32 (2012) 212-220.

[22] Q. Liu, Zhao, M. & Wang, L, Scattering of plane P, SV or Rayleigh waves by a shallow lined tunnel in an elastic half space, Soil Dynamics and Earthquake Engineering, 49 (2013) 52-63.

[23] Q. Liu, Zhao, M. & Zhang, C, Antiplane scattering of SH waves by a circular cavity in an exponentially graded half space, International Journal of Engineering Science, 78 (2014) 61-72.

[24] C. Yi, Zhang, P. & Johansson, D., Dynamic response of a circular lined tunnel with an imperfect interface., Computers and Geotechnics, 55 (2014) 165-171.

[25] C. Zhou, Hu, C., Ma, F. & Liu, D, Elastic wave scattering and dynamic stress concentrations in exponential graded materials with two elliptic holes, Wave Motion, 51(3) (2014) 466-475.

[26] M. Trifunac, Lee, V., Liu, W. & Orbovic, N, Scattering

and diffraction of earthquake motions in irregular, elastic layers, II: Rayleigh and body P and SV waves, Soil Dynamics and Earthquake Engineering, 66 (2014) 220-230.

[27] W. Vincent, Liu, W. Y, Two-dimensional scattering and diffraction of P-and SV-waves around a semi-circular canyon in an elastic half-space: An analytic solution via a stress-free wave function, Soil Dynamics and Earthquake Engineering, 63 (2014) 110-119.

[28] T.N. Akhlaghi, A., Effect of Vertically Propagating Shear Waves on Seismic Behavior of Circular Tunnels, The Scientific World Journal, 2014 (2014).

[29] H. Alielahi, Kamalian, M. & Adampira, M, Seismic ground amplification by unlined tunnels subjected to vertically propagating SV and P waves using BEM, Soil Dynamics and Earthquake Engineering, 71 (2015) 63-79.

[30] S.C. Lee, Evanescent wave scattering at off-axis incidence on multiple cylinders located near a surface. , Journal of Quantitative Spectroscopy and Radiative Transfer, 151 (2015) 239-250.

[31] H.R. Vosoughifar, Madadi, F. & Rabiefar, A, Modified Dynamic Stress Concentration Factor for Twin Tunnels Using a Novel Approach of FEM-Scattering, Tunnelling and Underground Space Technology, 70 (2017) 30-41.

[32] L. Huang, Liu, Z., Wu, C. & Liang, J., The scattering of plane P, SV waves by twin lining tunnels with imperfect interfaces embedded in an elastic half-space, Tunnelling, and Underground Space Technology, 85 (2019) 319-330.

[33] Q. Liu, Zhao, M. & Lio, Z., Wave function expansion method for the scattering of SH waves by two symmetrical circular cavities in two bonded exponentially graded half spaces, Engineering Analysis with Boundary Elements, 106 (2019) 389-396.

[34] M. Tao, Zhao, H., Li, Z. & Zhu, J, Analytical and numerical study of a circular cavity subjected to plane and cylindrical P-wave scattering, Tunnelling and Underground Space Technology, 95 (2020) 103-143.

[35] H. Vosoughifar, Modifying a circular analysis method for considering the scattering of earthquake waves in an opening in rock, in: 4th International Conference on Earthquake Geotechnical Engineering, Greece, 2007.

[36] M.S. Abramowitz, I., Handbook of mathematical functions, Washington, DC: National Bureau of Standards., 1964.

[37] ICSR, The Iranian code of practice for seismic resistant design of building (Standard NO.2800-5) Fourth Edition, Road, Housing & Urban Development Research Center, Tehran., 2013.

[38] F. Naeim, The Seismic Design Handbook (Volum1), PEER, 2001.

[39] D.H. Manoochehri, Shiraz City Historic city of Iran., 2015.

[40] F.E. Package, Finite element Package for Analysis of Geotechnical Structures, Delft, Netherland, 2002.

[41] T. Bourbie, Coussy, O. & Zinszner, B, Acoustics of porous media, Hoston: Golf Publishing., 1987.

HOW TO CITE THIS ARTICLE

A. Rabiefar, H.R. Vosoughifar, A. Nabizadeh, H. Negahdar, Modified Dynamic Stress Concentration Factor for the Scattering of P-wave by Twin Tunnels, AUT J. Civil Eng., 5(3) (2021) 433-448.

DOI: 10.22060/ajce.2022.19395.5729